An Image Processing Techniques Used for Soil Moisture Inspection and Classification

Mansur. AS[1], Herkules Abdullah[2], Hermawan Syahputra[3], Brahim Benaissa[4] , and Fauziyah Harahap[5]

{asmansur@unimed.ac.id[1], abdullahherkules@gmail.com[2], hsyahputra@unimed.ac.id[3]}

Department of Computer Sciences[1, 3], Department of Biology [2,5], Faculty of Mathematic and Natural Science, Universitas Negeri Medan, Indonesia
Toyota Technological Institute, Department of Mechanical Systems Engineering, Design Engineering Lab, Japan[4]

Abstract. A soil inspection provides information on the soil's fertility, an important starting point for determining soil fertility. Therefore, soil quality determination is essential in agricultural systems before planting. Image processing techniques associated with the computer vision model are widely used today, having applications in many branches of agriculture, closely related to technologies used in precision farming. This research aims to created an accurate model in image processing approaches for checking and categorizing soil quality based on external data detection. The visible and invisible strategies gathered using spectral technology were used to identify the exterior texture (computer vision). The Grey Level Co-occurrence Matrix (GLCM) approach was used to analyze picture texture, and then the Support Vector Machines (SVMs) method was used for classification. This study demonstrated that the model is an effective technique for evaluating soil moisture. Since the concealed texture features are not visible to the human eye, the experiment also shows that the invisible channels have promise in the classification model.

Keywords: images processing, classification, GLCM, SVMs, soil moisture.

1 Introduction

Agriculture is one of the most critical things in the world, including a strategic role in the growth of humankind. The essentials to grow harvest productivity, soil quality problems, or soil moisture handling has shown the use of modern farming approaches. Therefore, soil moisture is essential in agriculture, and plants may perish if there is a water deficit or oversupply. At the same time, this data is influenced by various external causes, most notably weather and climate change. That is why understanding the most effective methods for assessing soil moisture content is critical task. Even contemporary farmers have alternatives for monitoring soil moisture, such as sensors and sensing exterior textures.

In recent years, it has reported several benefits in image processing techniques related to soil, food assessments, and classifications. The image processing approach associated with computer vision and hyperspectral cameras has been widely chosen in the agricultural sector, especially

ICIESC 2022, October 11, Medan, Indonesia

DOI 10.4108/eai.11-10-2022.2325509

in soil moisture inspection to obtain quality grades [1-3], because they have excellent prospects and are very useful [2]. This technique is also straightforward to use and has a rapid inspection rate. The soil moisture, such as water strain, water fluctuations, and surface displacement or soil displacement field, is measured using instrumentation [10], and the water rate in the soil is calculated using an image processing approach. The proposed model is light speckle autocorrelation and observed membrane [3]. Black and white color imaging techniques are executed to decide the residue cover over the soil surface, and wavelength and filters are identified. They claim that imaging methodology proposed success in replacing human investigating fields [4][12][14].

Additionally, one inspection method used to estimate the water level of fruits and vegetables kept in various packing materials is hyperspectral imaging. The prediction maps, which display the model performance at the pixel level, were created from hyperspectral data. The study's findings demonstrate that hyperspectral imaging can be used to assess how various packing methods affect the water content of fruits and vegetables. Without touching the materials, the procedure allowed for a color examination duration of under a minute [7][17].

Next, the soil moisture is objectively evaluated in an investigation employing surface analysis based on curvelet transform. This examination stated that curvelet transforms textural components giving potential senses to estimate the water content of the soil [1-3]. The images were produced using a Charge Coupled Devices (CCD) coloring camera, and the investigation examined exterior textures. Furthermore, nearly earlier studies above indicated that surface image examination to quantify external texture differences from images is possible [9][14] because the image surface meditates the changes in intensity pixel significances, which may include information about the coloring and electromagnetic range of entities [6][9]. However, most of the techniques described above were designed to detect images exclusively from the visible range/spectrum (VS), such as RGB. Therefore that the whole variousness (heterogeneous) of colorings and surfaces is invisible, it will be challenging to apply [5,6] [14].On the other hand, it has been noted in several earlier investigations that the Near Infrared Spectroscopy (NIRS) technology used for the image processing approach still needs to be fully developed and faultless [4][9]. Moreover, the NIRS includes red-edge (invisible channel), an exciting technique introduced to visible range images to address the issue of image processing techniques on the RGB procedure [4,5]. The method, often known as a combination of visible and invisible channels, addresses challenges with image processing approach, such as restoration, augmentation, and identifying unseen pixels or concealed color texture [9].

Therefore, the initial goal of this work was to: first, investigate the features of soil moisture employing visible and invisible spectrum (channel), including image processing approaches such as image acquisition, image segmentation, and image feature extraction; second, use the Support Vector Machines (SVMs) method to classify soil moisture based on available water on the soil.

2 Data and Methodology

2.2 Data

The imaging contracted with the camera includes red, green, and blue (RGB) colors (visible) and channels infrared/IR (invisible). This combination aims to obtain global features for distortion-free images, including narrow bars of green, red, and blue for RGB images. The process is aligned with all visible and invisible images of the image pixels [6] [9]. The image was taken on both channels (visible and invisible) at the same time through the different optical paths with the aim for providing a distinct partition of the hidden and visible parts into five separate channelers, i.e., red (668 nm center, 10 nm bandwidth), green (560 nm center, 20 nm bandwidth), blue (475 nm center, 20 nm bandwidth), and IR (840 nm center, 40 nm bandwidth).

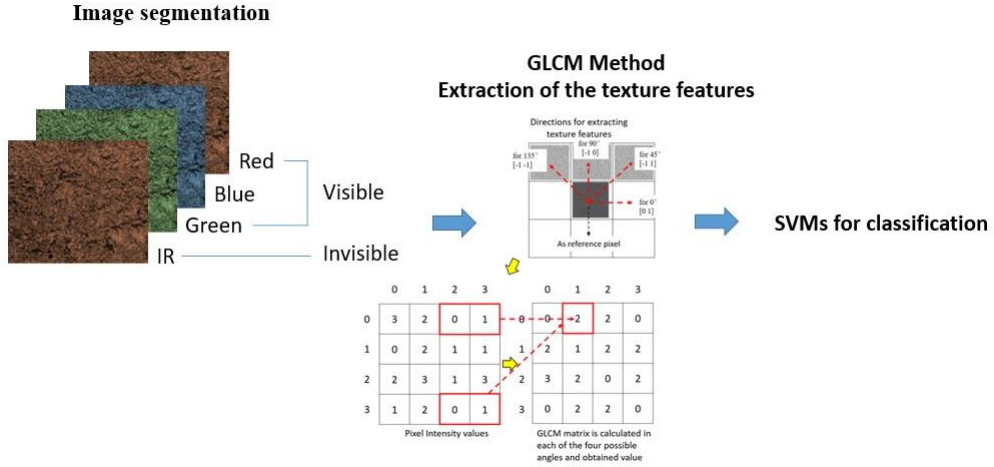

Fig. 1. Framework of experimental setup.

Next, the examination was carried out on two types of soil samples, i.e., andosol and alluvial soils, collected from Samosir Island, Indonesia. The maximum water content of the two types of soils is 45% due to all the available pore space on the soil having been served with water at that value. This soil is directed as being saturated due to the 45% volumetric water range; the soil can no longer carry water [17]. Additionally, to prevent the impact the numerous environmental elements, such as air movement and relative humidity, as well as the properties of the soil itself, which affect the swiftness at which water will permeate the soil, the soil were kept constant at 30 degrees temperature room. Next, the soil was put in front of the camera at the same spot and direction when taking pictures. A homogeneous lighting system and at 45 cm distance between the camera and the object were also maintained. In this work, for the first step, for every two types of soil, five images were taken at zero (0) hours, and in the next step, for every two types of soil, the five images were taken in each period, i.e., six hours, twelve hours, and twenty-four hours.

2.2 Methodology

Figure 1 shows the experimental procedure to examine the soil moisture. In the first step, the camera took images of two soil samples, and we next performed an image segmentation to remove avoided regions. Then an image acquisition technique employing the GLCM method was conducted by MATLAB Software (ver. R2019)., i.e., spectral data production and analysis. Finally, it is to classify the rate of moisture in each type of soil using the Support Vector Machines (SVMs) approach.

2.2.1 Image Segmentation

Since the picture contains an environment with pixels or textures representing an image's undesirable area, separating unwanted regions (background) from the scope of the appealing texture is required [15]. Generally, there are several processes termed image segmentation, and different techniques can be used, like edge-based segmentation (cropping), threshold-based segmentation, and color-based segmentation [6][8][13]. However, many previous studies suggested the segmentation technique is one model that is very easy to use and can improve promising results in the data analysis process.

Therefore, in this experiment, the cropping segmentation technique is utilized for the separate parts or sections of images, as illustrated in Figure 1. We next performed the texture and characteristics analysis, then the undesirable regions (background) of the picture were extracted, and the pixel (surface feature) value was black color (#0000) [15]. It represents the cropping segmentation technique that dramatically decreases the portion of data and filters out ineffective information while keeping the critical element of consistency features in the good parts [13,14].

2.2.2 Extraction of Texture Images

This work used the Gray-Level Co-occurrence matrix (GLCM) method for texture analysis. Gray-Level Co-occurrence matrix (GLCM) is an image texture analysis approach that denotes the association between two adjacent pixels with grayscale intensity, distance, and angle. Eight angles can be determined in GLCM, including angles 0 degrees, 45 degrees, 90 degrees, 135 degrees, 180 degrees, 225 degrees, 270 degrees, or 315 degrees. GLCM uses a two-dimensional matrix with the identical dimension as the number of gray levels in an image, namely a quadrangular matrix with specific properties; GLCM can indicate the spatial allocation of gray grades using pixels from the nearest neighbors in the surface image [9]. The equation of the co-occurrence matrix $CCM = C_{(Dx,Dy)}(N,M)$ as follows [11].

$$f(n) = CC_M^D(g_1, g_2) = \frac{1}{N.M}\sum_{n=1}^{N}\ \sum_{m=1}^{M} \qquad (1)$$

$$\begin{cases} 1 & if \quad I(n,m) = g_1 \quad 1 \quad I\left(n + D_x, m + D_y\right) = g_2 \\ 0 & otherwise, \end{cases}$$

, where $I(N,M)$ is an image of length, NxM is a location pixel (as a mentioned pixel), and while $D = (Dx,Dy)$ offset is described as $Dx = D.cos(\theta)$, $Dy = D.sin(\theta)$, where θ is the offset that determines the directive of the matrix from the central pixel $ncmc$ and D is the space from the

pixel central $n_c m_c$. Therefore, from the co-occurrence matrix CC_M and individually θ direction above, the contrast, correlation, energy, and homogeneity can be computed in equations (2), (3), (4) and (5) as follows [9][11].

$$\text{Contrast} = \sum_{i=1}^{G} \sum_{j=1}^{G} (i-j)^2 \, CC_M(i,j) \quad (2)$$

$$\mu_i = \frac{1}{N} \sum_{k=1}^{G} CC_M^D(i,k)$$

$$\mu_j = \frac{1}{M} \sum_{k=1}^{G} CC_M^D(k,j) \,,$$

$$\text{Correlation} = \frac{1}{G_x G_y} \sum_{i=1}^{G} \sum_{j=1}^{G} ij CC_M^D(i,j) - \mu_i \mu_j \,, \quad (3)$$

$$\text{Energy} = \sum_{i=1}^{G} \sum_{j=1}^{G} CC_M^D(i,j)^2, \quad (4)$$

$$\text{Homogeneity} = \sum_{i=1}^{G} \sum_{j=1}^{G} \frac{CC_M^D(i,j)}{1+|i-j|} \quad (5)$$

,where i = sum of pixels in the vertical direction, j = is the pixels in the horizontal direction, μ is the average of the likelihood matrix and σ is the standard deviations of the likelihood matrix. However, in our proposed approach, we determined just one neighboring pixel *D, (D = 1),* which are four possible spatial relationships (possible directions) as [0 1] for 0 degrees; [-1 1] for 45 degrees; [-1 0] for 90 degrees; [-1 -1] for 135 degrees.

Although the spatial association between two adjacent pixels can be determined in numerous methods with various offsets and angles [9], our work uses a default between the pixel and its nearest neighbor to its right [9]. We present four potential spatial associations characterized and executed, as illustrated in Figure 1.

2.2.3 Classification of the rate soil moisture

In this study, the pixel features i.e., contrast, correlation, energy, and homogeneity, that have been obtained from the GLCM method are calculated. Then those spectral feature values, including the standard deviation, the average, kurtosis, and skewness, were introduced as variables input (independent variables) in the Support Vector Machines (SVMs) method for classification. In this scenario SVMs was used to predict moisture in the soil (dependent variable) using features (independent variables). The approach was made with a mapping function of SVMs classification, which scenario is independent variables to predict the dependent variable. In contrast, the mapping function used in the SVMs method is a decision boundary that differentiates between two or more classes [18].

The SVMs configuration in Weka Software that we used is briefly described here. The class of hyperplanes $w.x) + b = 0$ $w \in RN$, $b \in R$, which correspond to the determination function $f(x) = sign((w.x) + b)$, is the foundation for SVMs classifiers. We can demonstrate that the hyperplane with the most significant margin of separation between the two categories is the ideal one. The actual use establishes the kernel procedure; the adaptation φ(.) is not specified explicitly. The

change φ(.) is determined by a kernel procedure *K(xi, xj)*, and its Eigenfunctions (an idea in practical analysis). It can be challenging to create eigen functions explicitly.

Here we shortly present the SVMs established in Weka Software that we used. SVMs classifiers are based on the category of hyperplanes, $(w.x) + b = 0$ $w \in RN$, $b \in R$, resembling decision procedures $f(x) = sign((w.x) + b)$. We can demonstrate that the optimal hyperplane is described as the one with the maximal margin of divergence between the two categories. In functional use, the establishes the kernel procedure; the change φ(.) is not explicitly declared. Provided a kernel procedure *K(xi, xj)*, the change $\varphi(.)$ is given by its Eigen procedures (an idea in the practical investigation). Eigenfunctions can be challenging to produce explicitly. Consequently, we define the kernel procedure without considering the precise adaptation. Thus, the Radial Basis Function (RBF) Network was used as the kernel procedure in this work. The hidden and output layers have highly different functions in the RBF procedure, and the corresponding weights also have quite diverse features. In addition, any of a variety of unsupervised learning approaches can be used to train (or set) the input to obscure weights, i.e., the basis procedure parameters $\{\mu ij, \sigma j\}$, in order to apply RBF in SVMs [11][18].

Next, we determine the kernel procedure without concern about the actual change. The Radial Basis Function (RBF) Network was chosen as the kernel procedure in this work. In the RBF function, the hidden and output layers recreate separate roles, and the corresponding weights have different meanings and properties. Thus, to use RBF in SVMs, the input to hidden weights (i.e., basis function parameters $\{\mu ij, \sigma j\}$ can be designed (or established) using any of a number of unsupervised learning approaches [11][18]. The hidden-to-output weights are then learned while the input-to-hidden weights are located and kept constant. Since there is only one layer of weights $\{wjk\}$ and only linear output activation procedures used in this second training phase, the weights can be efficiently determined analytically by solving a series of linear formulas. So, it can be completed fast without needing to perform a series of iterative weight updates, as in gradient descent learning [11].

3 Results and Discussion

3.1 Characteristics of Texture Images

In our approach, image processing techniques that combine visible and invisible channels are dependable when particular applications call for non-intrusive and non-contact methods (external inspection). To separate the elements consistently and reliably, each sample's characteristics are taken from its color vision and grouped for additional examination using the GLCM procedure. The GLCM method offers potential parameters for the analysis and computation of the fundamental properties of texture features [9].

To demonstrate the benefit of our suggested model and to catch transitions in surface features of the image in between time periods. The elements of the texture feature for visible channelers, i.e., blue, green, and red, and invisible channelers, i.e., IR, were analyzed as shown in Figures 2 and 3.

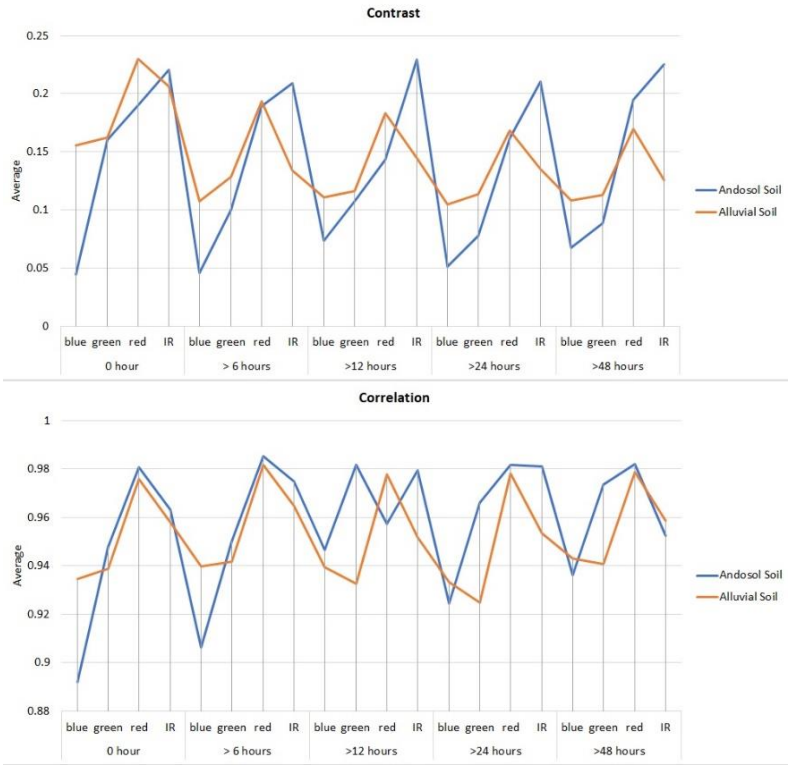

Fig. 2. The texture of contrast and correlation values across time periods.

As seen in Figures 2 and 3, there is a tendency for the average values of the texture feature contrast, correlation, energy, and homogeneity for visible and invisible categories to change over time. Additionally, distinct texture elements could be distinguished, particularly in the invisible channelers (IR), which provided excellent contrast values after period changes. These findings imply that the method has made it possible to analyze this soil in regions of the infrared range that are hidden from the human eye. Therefore, this technique made it possible to distinguish soil moisture that is not visual to human eyesight. These results demonstrated the necessity of accurately combining data from visible and invisible channelers to witness the external change for the two soil types.

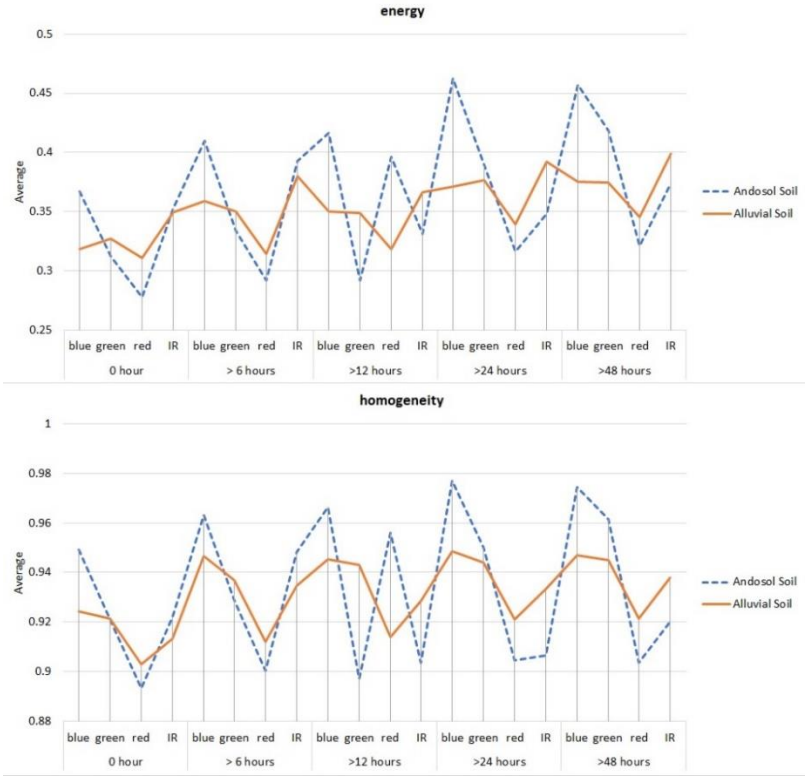

Fig. 3. The texture of energy and homogeneity values across time periods.

3.2 Change Over Time of The Characteristics Texture

To further our analysis, we compared texture changes from 0 hours to the between period. Next, the standard deviation of surface changes between periods was calculated separately for the channeler's texture feature. As illustrated in Table 1, for andosol soil in the visible channels, the results provided that a more increased value occurs on the contrast and energy texture in the green, blue and red channels. While for alluvial soil in the visual media, the contrast and correlation texture obtained increased values in the green and red channels. In addition, the more elevated value appears on the energy and homogeneity texture for invisible channels for andosol soil. Furthermore, a higher value for alluvial soil in the invisible channels also appears on the contrast and homogeneity texture.

Therefore, using the GLCM method, we argue that the visible and invisible channel delivers a helpful model to detect outer changes science does not see in the human eye, i.e., the IR channel. The integration of visible and invisible channels provides a better disparity of soil moisture change. So, we concluded that the co-occurrence analysis delivered a significant difference between periods for all textural features in both soils, including contrast, correlation, energy,

and homogeneity for five channels (visible and invisible). In addition, the results provided are definitive and can potentially categorize soil moisture.

Table 1. Standard deviation value

Channel	Contrast		Correlation		Energy		Homogeneity	
	Andosol	Alluvial	Andosol	Alluvial	Andosol	Alluvial	Andosol	Alluvial
blue	0.019	0.021	0.032	0.003	0.034	0.023	0.010	0.010
green	0.032	0.026	0.016	0.021	0.037	0.018	0.021	0.011
red	0.022	0.038	0.015	0.009	0.052	0.037	0.025	0.013
IR	0.009	0.034	0.008	0.006	0.026	0.018	0.020	0.010

3.2 Classify The Soil Moisture

The dataset is tested on two types of soil (andosol and alluvial), and two-dimensional GLCM is used, as was mentioned early in Section 2. Each test also had additional requirements, such as the minimum region size and the threshold value for the merge operation [9][16].

Next, soil moisture classification has been performed here with the SVMs method. Then, classify soil moisture rate according to period, i.e., ideal, average, fair, low, dry, and too dry. Then, we evaluated our proposed model's performance at classifying data using 10 k-fold cross-validations in the Weka Application and training and testing for subsets of the data.

Table 2. Result performance

Type of Soil	All Channels	RGB Channels	Invisible Channels
Alluvial	87.43%	79.36%	85.71%
Andosol	95.35%	87.36%	84.63%

The classification of soil moisture performance can be seen in Table 2. As can be seen, all channels achieved a classification of alluvial soil moisture of 87.43%, visible channels achieved a classification of 79.36%, and invisible channels achieved a higher performance of 85.71%. In addition, the classification of soil moisture using andosol soil obtained 95.35% overall, 87.36% for visible channels, and 84.63% for invisible channels.

This shows that the invisible channel successfully located the andosol soil's hidden texture features, which are not readily apparent to the human eye. The performance metric of texture data (textural elements) that have been acquired from the GLCM approach is calculated then those spectral components, including the standard deviation, mean, kurtosis, and skewness values were presented as variables input (independent variables) in Support Vector Machines (SVMs) method for classification the soil moisture.

For training and testing data for all channels, 250 images data were used. The results were all calculated: True Positive Rate (TPR), False Positive Rate (FPR), recall, and precision. Table 3 shows that for the classification of alluvial soil across all channels, the mean TPR for each type was 86.43%, the mean FPR was 3.41%, and the mean recall and precision were 87.62% and 86.41%, respectively. While the mean per-type true positive rate for the classification of andosol soil for all channels was 94.34%, the false positive rate was 1.34%, and the recall and precision were 94.50% and 94.34%, respectively.

Table 3 The metric performance

Type soil	True Positive Rate (%)	False Positive Rate (%)	Precision (%)	Recall (%)
Andosol	94.34	1.34	94.50	94.34
Alluvial	86.43	3.41	87.62	86.41

Based on the results, we identified all possible channels (both visible and invisible) for classifying soil moisture and produced positive classification outcomes. Therefore, as suggested by [9], using both visible and invisible channels can enhance the soil moisture category model in image processing approaches.

4 Conclusion

The gray-level pixels from nearest neighbors (GLCM) in the external surface image can be used to identify texture features precisely. The experimental results showed promising performance in classifying soil moisture using the Support Vector Machines (SVMs) method for the classification model.

Although the image's texture features can be undetectable utilizing a visual system like RGB, they are a fundamental function of visualization techniques. Nevertheless, the context of the color investigation should be considered a crucial element when combining visible and invisible approaches to correctly interpret the data analysis in image processing techniques.

The hereafter of image processing approaches involved in soil assessment is favorable, with agriculture technology becoming increasingly aware, analyzing, and managing variability in domains by conducting yield production practices at a suitable place and duration. This proposed model is an essential mechanism for the examination and control of the above parameters automatically. Therefore, our future work will be demanded to continue developing these approaches, creating a more rugged model that includes online techniques by employing a more significant type of soil with more comprehensive verification approaches.

Acknowledgments. This research was funded by Public Service Agency Fund (BLU) Universitas Negeri Medan, Indonesia, No. 0188/UN33.8/PPKM/PD/2022.

References

[1] Castaldi, Fabio, Angelo Palombo, Simone Pascucci, Stefano Pignatti, Federico Santini, and Raffaele Casa. "Reducing the influence of soil moisture on the estimation of clay from hyperspectral data: A case study using simulated PRISMA data." Remote Sensing 7, no. 11 (2015): 15561-15582.

[2] Saberioon, Mohammadmehdi, Asa Gholizadeh, Petr Cisar, Aliaksandr Pautsina, and Jan Urban. "Application of machine vision systems in aquaculture with emphasis on fish: state-of-the-art and key issues." Reviews in Aquaculture 9, no. 4 (2017): 369-387.

[3] Gachet, Philippe, Georg Klubertanz, Laurent Vulliet, and Lyesse Laloui. "Interfacial behavior of unsaturated soil with small-scale models and use of image processing techniques." Geotechnical Testing Journal 26, no. 1 (2003): 12-21.

[4] Jin, Xiuliang, Jianhang Ma, Zhidan Wen, and Kaishan Song. "Estimation of maize residue cover using Landsat-8 OLI image spectral information and textural features." Remote Sensing 7, no. 11 (2015): 14559-14575.

[5] Liu, Yuwei, Hongbin Pu, and Da-Wen Sun. "Hyperspectral imaging technique for evaluating food quality and safety during various processes: A review of recent applications." Trends in food science & technology 69 (2017): 25-35.

[6] Cubero, Sergio, et al. "Advances in machine vision applications for automatic inspection and quality evaluation of fruits and vegetables." Food and bioprocess technology 4.4 (2011): 487-504.

[7] Handa, Takemi, Rajesh G. Katare, Hideaki Nishimori, Seiichiro Wariishi, Takashi Fukutomi, Masaki Yamamoto, Shiro Sasaguri, and Takayuki Sato. "New device for intraoperative graft assessment: HyperEye charge-coupled device camera system." General thoracic and cardiovascular surgery 58, no. 2 (2010): 68-77.

[8] Tang, Tiantian, Min Zhang, and Arun S. Mujumdar. "Intelligent detection for fresh-cut fruit and vegetable processing: Imaging technology." Comprehensive Reviews in Food Science and Food Safety (2022).

[9] Parewai, Ismail, Mansur As, Tsunenori Mine, and Mario Koeppen. "Identification and classification of sashimi food using multispectral technology." In Proceedings of the 2020 2nd Asia Pacific Information Technology Conference, pp. 66-72. 2020.

[10] Sirimorok, Nurdiansyah, Mansur As, Kaori Yoshida, and Mario Köppen. "Smart Watering System Based on Framework of Low-Bandwidth Distributed Applications (LBDA) in Cloud Computing." In International Conference on Intelligent Networking and Collaborative Systems, pp. 447-459. Springer, Cham, 2020.

[11] As, Mansur, Hiroshi Shimizu, Brahim Benaissa, Kaori Yoshida, and Mario Köppen. "Calibration Cost Reduction of Indoor Localization Using Bluetooth Low Energy Beacon." Journal of Advanced Computational Intelligence and Intelligent Informatics 26, no. 1 (2022): 97-106.

[12] Hasinoff, Samuel W. "Saturation (imaging)." In Computer Vision: A Reference Guide, pp. 1107-1109. Cham: Springer International Publishing, 2021.

[13] Su, Wen-Hao. "Advanced Machine Learning in Point Spectroscopy, RGB-and hyperspectral-imaging for automatic discriminations of crops and weeds: A review." Smart Cities 3, no. 3 (2020): 767-792.

[14] Domino, Małgorzata, Marta Borowska, Natalia Kozłowska, Anna Trojakowska, Łukasz Zdrojkowski, Tomasz Jasiński, Graham Smyth, and Małgorzata Maśko. "Selection of image texture analysis and color model in the advanced image processing of thermal images of horses following exercise." Animals 12, no. 4 (2022): 444.

[15] Rajitha, B., & Agarwal, S. (2022). Segmentation of Epiphysis Region-of-Interest (EROI) using texture analysis and clustering method for hand bone age assessment. Multimedia Tools and Applications, 81(1), 1029-1054.
[16] As, Mansur, and Tsunenori Mine. "Prediction of Travel Time over Unstable Intervals Between Adjacent Bus Stops Using Historical Travel Time in Both the Previous and Current Time Periods." In Intelligent Transport Systems for Everyone's Mobility, pp. 131-153. Springer, Singapore, 2019.
[17] Lehmann, Peter, Francesca Gambazzi, Barbara Suski, Ludovic Baron, Amin Askarinejad, Sarah M. Springman, Klaus Holliger, and Dani Or. "Evolution of soil wetting patterns preceding a hydrologically induced landslide inferred from electrical resistivity survey and point measurements of volumetric water content and pore water pressure." Water Resources Research 49, no. 12 (2013): 7992-8004.
[18] Srunitha, K., and S. Padmavathi. "Performance of SVM classifier for image based soil classification." In 2016 International Conference on Signal Processing, Communication, Power and Embedded System (SCOPES), pp. 411-415. IEEE, 2016.